WPPFC-CPR(17) 17076

A Eksaeva et al.

ERO modelling of experiments on Cr sputtering at linear plasma device PSI-2

Preprint of Paper to be submitted for publication in Proceeding of 16th International Conference on Plasma-Facing Materials and Components for Fusion Applications

This work has been carried out within the framework of the EUROfusion Consortium and has received funding from the Euratom research and training programme 2014-2018 under grant agreement No 633053. The views and opinions expressed herein do not necessarily reflect those of the European Commission.

ERO modelling of Cr sputtering in the linear plasma device PSI-2

A. Eksaeva[1,2], D. Borodin[1], A. Kreter[1], D. Nishijima[3], A. Pospieszczyk[1], T. Schlummer[1], S. Ertmer[1], A.Terra[1], B. Unterberg[1], A. Kirschner[1], J. Romazanov[1], S. Brezinsek[1], M.Rasinski[1], S. Henderson[4], M. O'Mullane[4], H. Summers[4], M. Bluteau[4], E. Marenkov[2]

[1]*Forschungszentrum Jülich GmbH, Institut für Energie- und Klimaforschung – Plasmaphysik, Partner of the Trilateral Euregio Cluster (TEC), 52425 Jülich, Germany*

[2]*National Research Nuclear University MEPhI, 31, Kashirskoe sh., 115409, Moscow, Russia*

[3]*Center for Energy Research, UC at San Diego, 9500 Gilman Dr., La Jolla, CA, 92093-0417, USA*

[4]*Department of Physics, University of Strathclyde, Glasgow G4 0NG, UK*

Key words: PSI-2, erosion, physical sputtering, chromium, spectroscopy

Abstract

Chromium (Cr) is a fusion-relevant reactor wall element (e.g. component of RAFM steels expected for use in DEMO). Linear plasma devices including PSI-2 are effective tools for investigations of plasma-surface interaction effects, allowing continuous plasma operation for tokamak divertor relevant conditions. Experiments on Cr sputtering were conducted at PSI-2. In these experiments the Cr erosion was measured by three techniques: mass loss of the sample, quartz micro-balance of deposited impurities at a distance from it and optical emission spectroscopy. Experiments were modelled with the 3D Monte-Carlo code ERO, previously validated on similar experiments with tungsten. The simulation results are in a good agreement with the experiment. Initial population of metastable levels was fitted by matching the modelling with the experiment. The usage of ADAS atomic data have shown to result in a good agreement with the experiment if the initial population of metastable states after sputtering is taken into account.

I. Introduction

Plasma interaction with the first wall (FW) materials is one of the critical questions for the development of the fusion reactor technology including the upcoming tokamak ITER [1]. For instance, FW erosion limits plasma-facing component (PFC) lifetime. Physical sputtering of the FW components can cause significant plasma contamination and subsequent energy losses through the radiation of ionized impurities. Reliable prediction of the sputtering source and resulting material influx into the plasma and its further transport towards the plasma core is indispensable. Chromium (Cr) is a component of RAFM steels [2], a primary candidate alloy for the first chamber wall of the DEMO fusion reactor prototype [3]. Moreover, the similarity in electron structure of Cr with tungsten (W), which is the main material for the divertor area of ITER and molybdenum can also serve for development and validation of the atomic data useful for diagnostic of all three potential plasma impurities.

Linear plasma devices, such as PSI-2 [4], PISCES-B [5], PR-2 [6] are excellent test beds for the investigation of plasma-surface interaction (PSI) due to continuous plasma operation. The PSI-2 facility is capable of simulating main discharge parameters relevant for divertor area of tokamaks [7].

The initial population of metastable (MS) levels of sputtered atoms has a significant influence on both the impurity line emission intensity and line ratios values. Several investigations have shown the significance of this effect [8, 9, 10], however, so far there is still no detailed description of the influence of the sputtering process on the energy levels population distribution just after the sputtering event. This effect is specific for various atoms and ions. Another relevant effect is surface morphology often evolving during the plasma exposure, which can have a large influence on the sputtering yield and angular distribution of sputtered particles [10, 11, 12]. In its turn, the angular distribution of sputtered particles has the most significant influence on the penetration depth of sputtered particles. Therefore, numerical modeling is indispensable for the correct interpretation of experiments in linear plasma devices and subsequent extrapolation of results to ITER and DEMO.

The 3D Monte-Carlo ERO code [13] is a tool for modelling the impurity transport in fusion devices. ERO calculates the PSI and 3D impurity transport in plasma in the test particle approximation and takes into account a wide range of physical processes: ionization, recombination, light emission, Lorentz force, friction and thermal forces. elastic collisions, metastable population evolution, etc. In this work experiments on Cr sputtering with Neon (Ne) and Helium (He) plasmas were modelled with the ERO code. Matching of modelling with the experiment was used for validation of MS-resolved atomic

data from ADAS [14, 15] (new ADAS'17 dataset for photon-emission coefficients (PEC) and ionization/excitation data) used in the ERO code.

II. Experiments

The PSI-2 is a linear plasma device of approximately 3 meters length with a magnetically confined plasma column of ~6cm in diameter. The axial magnetic field in the facility is about 0.1 T varying along the device due to magnetic coils configuration. The range of possible exposure parameters covers expected conditions in ITER. The facility produces ion fluxes to the target in the range of 10^{21}-10^{23} $m^{-2}s^{-1}$, with electron densities n_e = 10^{17}-10^{19} m^{-3} and temperatures T_e = 3-20 eV. The sample temperature can be varied from 400 to 1400 K. An appropriate value of fluence (10^{23}-10^{27} m^{-2}) can be reached by extending the exposure time. The magnetic field is normal to the target surface. The plasma source cathode has a cylindrical shape. Therefore, radial plasma profiles have a hollow shape, with a minimum on the facility axis for both plasma density and temperature. A detailed description of the facility can be found elsewhere [4,16].

Fig. 1 illustrates the scheme of the PSI-2 device (fig. 1a) and the conducted Cr erosion experiment configuration (fig. 1b). The experiment was similar to the W sputtering experiments described in an earlier work [9].

In the experiments a Cr target of size 80x100 mm^2 with 10 5x5 mm^2 imbedded samples (fig.1b) was irradiated by Ne and He plasmas. 10 samples from the target were used for individual mass loss measurements, thus, providing spatial resolution. A negative biasing voltage U_b was applied to the target, controlling the energies of incident plasma ions. The electron density n_e and temperature T_e were measured with a reciprocating Langmuir probe at approximately 310 mm away from the target surface along the z-axis. At the radial position of the maximum flux the parameters of He plasma were n_e = (5-7)×10^{11} cm^{-3} and T_e = 5-6 eV, and of Ne plasma n_e = (2-3)×10^{11} cm^{-3}, T_e = 5-6 eV. The conducted experiments and their parameters are listed in Table 1. Some difference of erosion process in Ne and He plasmas was expected due to surface morphology evolution in the latter case.

Table 1. Cr physical sputtering experiments conducted at PSI-2 facility.

	Plasma	Exposure parameters	Measurements
1	He	N_e = (7-8)×$10^{11}$$cm^{-3}$ T_e = 5-6 eV E_{in} ≈ 100eV	• Mass loss • Spectroscopy along the facility axis
2	Ne	N_e = (2-3)×$10^{11}$$cm^{-3}$ T_e=5-6 eV E_{in} ≈ 100eV	
3	He	N_e = (3-7)×$10^{11}$$cm^{-3}$ T_e = 5-6 eV E_{in} ≈ 150eV	• QMB-target axial position (distance from the target) scan
4	Ne	N_e = (2-3)×$10^{11}$$cm^{-3}$ T_e = 5-6 eV E_{in} ≈ 40-160 eV	• QMB signal as a function of U_b

The quartz microbalance sensor (QMB) was installed at a distance from the movable target outside the plasma column and served as a witness plate during the experiments. The QMB sensor measures the amount of target material reaching its surface; the diameter of the sensor is 8 mm. The QMB allows *in situ* measurement of the angular distributions of sputtered particles by changing its axial position with respect to the target. The scan of the axial target position (relative to QMB) was conducted in the beginning and in the end of the exposure for the experiment #3 from Table 1. The axial distance was varied from 20 to 540 mm. These two scans were expected to reveal changes in angular distributions of sputtered particles due to morphology evolution. To study the influence of the ion impact energy on the Cr erosion, also the scan of QMB signal in dependence on the target U_b was conducted for the Ne plasma irradiation (experiment #4, Table 1).

Cr I 520.8 nm (a^5S - $z^5P°$) and Cr I 427.0 nm (a^7S - $z^7P°$) line intensity profiles along the facility axis were measured by optical emission spectroscopy 0-50 mm in front of the target. The 427.0 nm line is the ground-state driven transition;

whereas the 520.8nm line is populated from the MS state ^5S (see the Grotrian diagram depicted in fig.2). Here we don't consider possibility of excitation of the above lines through cascades and assume it to be negligible in comparison with excitation from the lower level of the transition.

After the experiment scanning electron microscopy (SEM) analysis of the samples was conducted. The surface morphology evolution influence on the sputtering process was observed through changes in the QMB signal for the He plasma irradiation. In the He irradiation case sputtering intensity has decreased by 20% after ≈3.5 hour exposure (see fig.3). However, SEM analysis revealed only relatively small changes in surface morphology (see fig.4) with rare unevenly distributed structures. The developed structures are mostly cones. The density of the structures seemed too low to affect the sputtering intensity to such an extent. Therefore, the reason for the sputtering intensity decrease is still under investigation. The surface was polished before the exposure; however, there is a possibility that the upper layer was eroded in a larger rate than the subsequent layers due to defects of the crystalline structure. More detailed investigation of the polished surface is needed. For the Ne plasma irradiations the QMB signal was constant and much less morphology changes on the surface were observed.

III. Modelling methods and assumptions

The 3D Monte-Carlo ERO code calculates PSI and impurity transport in the test particles approximation. The amount of sputtered material is calculated with yields according to the Eckstein approximation formula [17]. The fits are based on binary-collision approximation (BCA) SDTrimSP code simulations. In ERO simulations the area of the target surface is divided into rectangular surface cells. The amount of particles starting from every surface cell (1x1mm^2) is 100, which leads to the full number of particles in simulation 8x10^5. Initial velocities and angles for test particles starting from each cell are generated based on known distributions discussed in [9], however the angular distribution for sputtered Cr is also part of the current study. Elementary processes (i.e. ionization, recombination, elastic collisions) are treated with the Monte-Carlo method based on reaction rates from ADAS [14]. The ionization, recombination, GS-MS transitions coefficients are taken from the recent ADAS dataset for Cr I [15]. Ion friction with the plasma flow, diffusion and thermal forces are taken into account. Self-sputtering by ERO-tracked particles returning to the surface is also included. The line emission intensity value for every volume cell is calculated according to:

$$I = PEC(n_e,T_e)\cdot n_e\cdot n_{imp} \quad (1)$$

where PEC is the photon emission coefficient [cm^3/s], and n_e, T_e, n_{imp} are correspondingly local electron density, electron temperature and impurity concentration. ERO provides integration of the emission intensity along the given line of sight, thereby synthesizing the spectrometer view.

Evolution of metastable levels population is tracked assuming a system of one ground $^7S_3$ (GS) and one metastable $^5S_2$ (MS) level similar to the way it was done earlier for Be [8]. Most excitation-relaxation processes affecting the observed lines are assumed to be much faster than the MS-GS population evolution. The QMB sensor measurements are also simulated in the code.

Plasma parameters in the volume are on the basis of probe measurements with the radial resolution. In the axial direction the electron density n_e is assumed to decrease to the target surface according the Stangeby free-flow model, which showed to be a good approximation for linear plasma devices [18]. T_e is assumed to be constant along the facility axis. The ERO simulation box has a size of 400x400x600 mm^3.

IV. Results and discussion

Four experimental observations (including the trends during parameter scans) were modelled with ERO:

- Mass loss measurements
- QMB signal as a function of target bias voltage U_b (for Ne plasma irradiation)
- QMB signal as a function of axial distance from the target (for the He plasma irradiation)
- Cr axial spectroscopy profiles (λ = 420 nm and λ = 520.8 nm)

In the current work we largely use the experience of the previous work on W sputtering simulation [9], which has allowed validating basic assumptions of the modelling. Atomic data used in the code for ionization, excitation and photon emission calculations are quite sensitive for T_e in the range of T_e < 10eV. The uncertainty of Langmuir probe measurements

for T_e is about 1-1.5 eV. To investigate the influence of uncertainties in T_e the sensitivity studies were performed assuming T_e different from the measured value by ±50%. QMB measurements have shown a weak dependence on these variations, whereas spectroscopic measurements conducted just near the target surface strongly reflect the changes. The best agreement for all ERO trends simultaneously was observed when T_e was increased by 50%, while n_e is decreased by 50%. The effective connection length [18] determining the n_e fall towards the target was fitted from previous experiments at PSI-2 to be about 1000 mm. It should be noted, that the fitting was done only for the axial target position l = 345 mm relative to the QMB sensor, whereas later on position scans like in the experiment #3 (see Table 1) can affect the connection length and thereby the n_e value just near the target surface. Therefore, in the experiment #3 plasma parameters were measured with the Langmuir probe for every target position.

Furthermore, it is well known that in linear plasma devices a fraction of high-energy non-Maxwellian electrons can be present [19]. It can have a significant influence on the calculated ionization and excitation rates; however the accustomed Maxwellian averaged values were used in the simulations, because in [20] it is shown that for the parameter range under consideration in PSI-2 this effect is negligible. The expected time-averaged fraction of suprathermal electrons in plasma was shown to be $<n_{st}>/n_e \approx 10^{-8}$.

Modelling results of mass loss measurements are presented in fig.4. One can see that in general the modelled results are in a good agreement with the experiment, meaning confirmation of the SDTrimSP-simulated sputtering yields by the measurement. Re-deposition is taken into account in the ERO modelling, therefore direct comparison with the experimental net erosion values is justified. For the case of Ne plasma irradiation the re-deposition fraction estimated with ERO was 6%, and 14% for the case of He irradiation. Prompt re-deposition in both cases was less than 1%. A bit more pronounced discrepancy between ERO mass loss simulations and measurements can be seen for the He irradiation case. This can be attributed to the evolving surface morphology, which suppresses the sputtering process. The morphology evolution was observed via the QMB signal, which has shown a decrease of the Cr erosion by 20% during the irradiation in He plasma (see fig.5). Incorporation of the morphology evolution into ERO is under development.

ERO-modelled QMB signals are presented in fig. 6a as function of the target biasing voltage for Ne plasma irradiation. One can see the good qualitative and quantitative agreement. For He plasma the QMB signal as a function of the axial distance from the target surface was obtained (see fig. 6b). ERO modeling is in a good quantitative agreement; however the maximum position differs from the experiment. This is most likely due to uncertainties in the n_e decay to the target, in particular at small distances from it. The experimental signal decreased by 20% in the process of irradiation, probably due to the surface morphology evolution (see the results at fig.6, in the beginning and at the end of irradiation), however the maximum position did not change: this indicates negligible changes in the angular distribution of the sputtered particles. That is an expected result, taking into account rare and unevenly distributed morphology structures on the surface.

The ERO-simulated axial intensity profiles for the Cr I λ = 520.8 nm ($a^5S - z^5P°$) and λ = 427.0nm ($a^7S - z^7P°$) lines are shown in the fig.7. These lines were selected for measurement and modelling because of fundamental difference in their population mechanism. The line λ=427.0 nm is mainly populated by the excitation from the ground-state.; It can be expected to have the highest intensity just near the target surface. In a contrast, the λ=520.8 nm line is mostly excited from the MS state (we don't take cascades as a possible way of the line's excitation into consideration). Thus, some time is needed for the population of the corresponding MS level (relaxation up to equilibrium determined by the plasma conditions) and, therefore for radiation intensity increases (see fig.2), which results in a radiation intensity maximum at some distance from the target surface. In the fig.7 one can see a good qualitative agreement between the modelling and the experiment. Absolute values are in agreement by an order of magnitude.

Good agreement for the mass loss measurements and deposition at QMB during the target position scans indicate that the ERO transport model, including the initial angular distribution of sputtered particles is correct. Therefore the only uncertain parameter for the spectroscopy measurements is the initial population of MS states. Initial population of MS levels was fitted by matching the experimental relative line intensities with the ERO simulations as 6% MS for He irradiation and 15% MS for the Ne plasma irradiation. The reason for the difference in the initial MS population is under investigation. Further experiments at PSI-2 on Mo sputtering and subsequent Cr-Mo-W atomic data validation are planned.

V. Summary

The numerical modelling using 3D Monte-Carlo code ERO is shown to be useful for the interpretation of the erosion (physical sputtering) experiments conducted in linear plasma devices like PSI-2. In this work a series of experiments on Cr sputtering was simulated with ERO as a continuation of the previous similar experiments on W erosion.

Surface morphology evolution under He plasma irradiation was observed. The developed morphology is probably responsible for the decrease of sputtering yield by 20%, however it had no significant influence on the angular distribution of sputtered particles due to uneven distribution of morphology structures. During the same experiment for Ne the signal decrease was not observed.

A good agreement between the modelling and the experiment is observed for both mass loss and QMB re-deposition measurements. The recent ADAS set of MS-resolved atomic data for Cr was used in the calculations and was shown to be in a good agreement with the experiment. The initial MS population of sputtered atoms was fitted from matching of ERO spectroscopy modelling with the experimental line ratios: 6% MS for He irradiation and 15% MS for the Ne irradiation.

Chromium, molybdenum (Mo) and tungsten have similar electronic structures [15], which can facilitate calculation and validation of atomic data for tungsten making this work the first step in the larger investigation. In the frame of this similar experiments with ERO interpretation at PSI-2 are also planned for Mo.

VI. Acknowledgments

The work is supported by the EUROfusion WP PFC.

This work has been carried out within the framework of the EUROfusion Consortium and has received funding from the Euratom research and training programme 2014-2018 under grant agreement No 633053. The views and opinions expressed herein do not necessarily reflect those of the European Commission.

References

[1] Pitts, R. A., et al. (2011). Journal of Nuclear Materials, 415(1), S957-S964.
[2] Lucon, E., et al. (2006). Fusion engineering and design, 81(8), 917-923.
[3] Boccaccini, L. V., et al. (2004). Journal of Nuclear Materials, 329, 148-155.
[4] Kreter, A., et al. (2015). Fus. Sci. and Tech., 68(1), 8-14.
[5] R.P. Doerner , et al. , Nucl. Fus. 52 (2012) 103003 . [6] Gutorov, K. M., et al. (2016). Journal of Surface Investigation. X-ray, Synchrotron and Neutron Techniques, 10(3), 612-616.
[7] Kreter, A. (2011). Fus. Sci. and Tech., 59(1T), 51-56.
[8] D. Borodin , et al. , in: 36th EPS Conference on Plasma Phys. Sofia, 2009 ECA, 33, 2009, p. 5.197
[9] A. Eksaeva, et al., Nucl. Mater. Energy (2017), doi: 10.1016/j.nme.2017.03.014
[10] D. Borodin et al., Nucl. Mater. Energy (2017), doi: 10.1016/j.nme.2017.05.004
[11] Doerner, R. P., et al. (2014). Phys. Scr., 2014(T159), 014040.
[12] Kurnaev, V. et al. (2003). Physica Scripta, 2003(T103), 85..
[13] Kirschner, A., et al. (2007). J. of Nuc. Mat., 363, 91-95.
[14] Summers, H. P., & O'Mullane, M. G. (2000, November). The atomic data and analysis structure. In K. A. Berrington, & K. L. Bell (Eds.), AIP Conference Proceedings (Vol. 543, No. 1, pp. 304-312). AIP.
[15] Badnell, N. R., et al. (1996). Journal of Physics B: Atomic, Molecular and Optical Physics, 29(16), 3683.
[16] M. Reinhart et al., Trans. Fusion Sci. Technol. 63 (2013) 201.
[17] Eckstein, W. (2007). Sputtering yields. In Sputtering by Particle Bombardment (pp. 33-187). Springer Berlin Heidelberg.
[18] LaBombard, B., et al. (1989). Journal of Nuclear Materials, 162, 314-321.
[19] Waldmann O and Fussmann G 2006 ECA - EPS Proc. 30 I P-1.049
[20] Waldmann, O., et al. (2010). Plasma Sources Science and Technology, 19(4), 045007.

Figures

a)

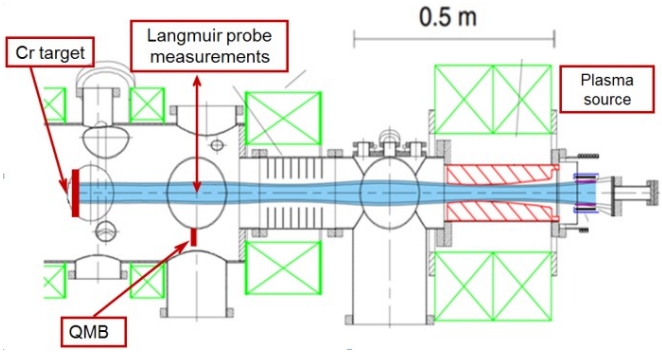

b)

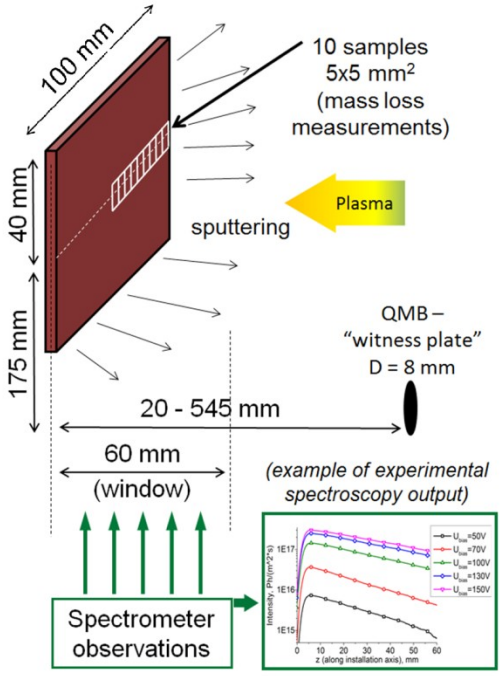

Fig.1. a) Scheme of the PSI-2 facility; b) scheme of the experiments and used diagnostics.

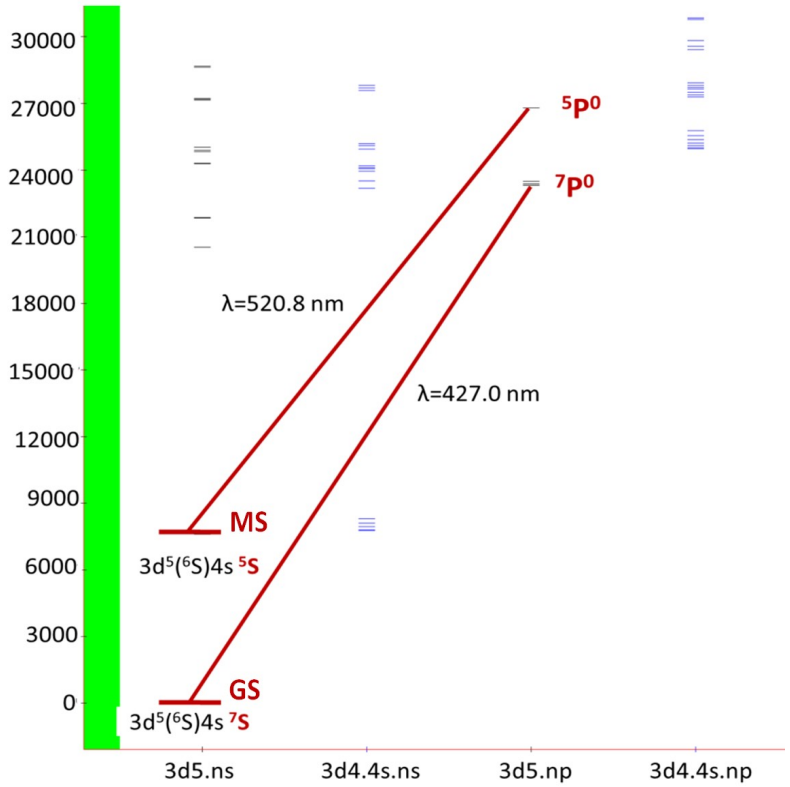

Fig.2. Energy levels of Cr and main observed transitions (λ = 520.8 nm (a^5S - $z^{5P°}$) and λ = 427.0nm (a^7S - $z^7P°$)).

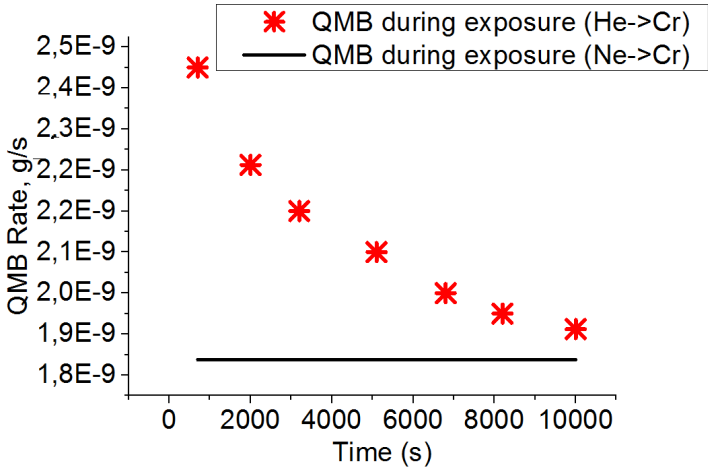

Fig.3. Deposition rate on QMB as a function of the irradiation time (He and Ne irradiation, E_{in} ≈ 100 eV).

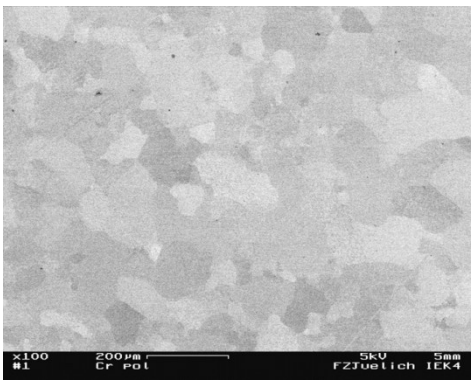

a)

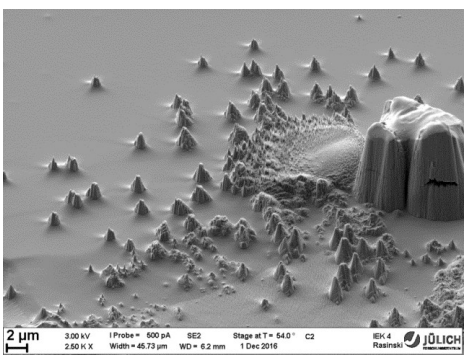

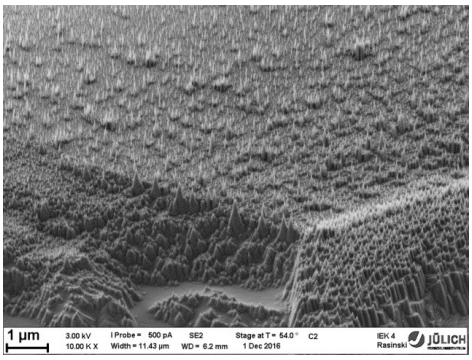

b)

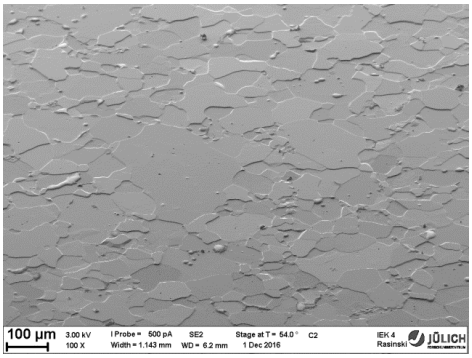

c)

Fig.4. SEM analysis of Cr samples a) before and b) c) after the He plasma exposure on a) small scale b) large scale.

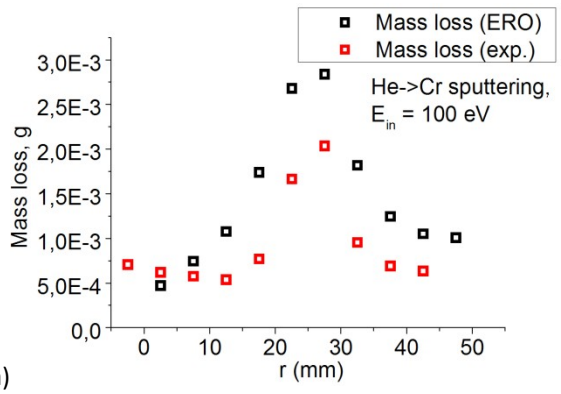

a)

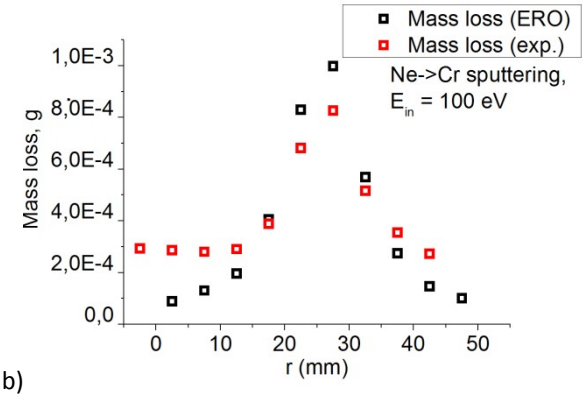

b)

Fig.5. Mass loss measurements from the experiments in comparison with the ERO modeling;
a) He plasma irradiation, $E_{in} \approx 100$ eV; b) Ne plasma irradiation, $E_{in} \approx 100$ eV.

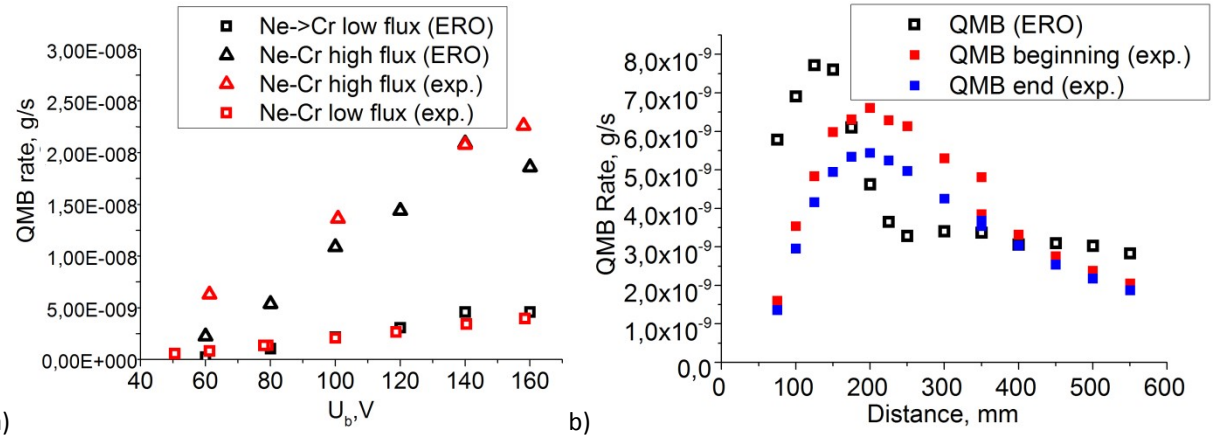

Fig.6. a) Ne plasma irradiation, experiment #4. QMB signal as a function of E_{in};
b) He plasma irradiation, experiment #3 (table 1), QMB signal as a function of the axial distance from the target surface.

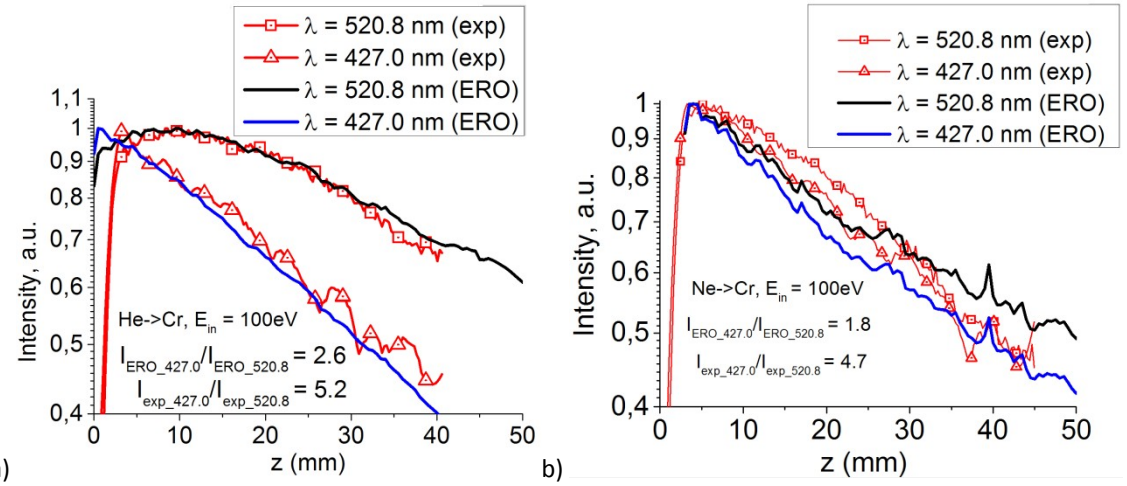

Fig.7. Cr I line emission intensity profiles along the facility axis for C I λ = 520.8 nm and λ = 427.0 nm lines;
a) He plasma irradiation, $E_{in} \approx 100$ eV; b) Ne plasma irradiation, $E_{in} \approx 100$ eV.